Ute A. Hellmich, Benjamin L. Weis, Anatoli Lioutikov, Jan Philip Wurm, Marco Kaiser, Nina A. Christ, Katharina Hantke, Peter Kötter, Karl-Dieter Entian, Enrico Schleiff and Jens Wöhnert

Essential ribosome assembly factor Fap7 regulates a hierarchy of RNA-protein interactions during small ribosomal subunit biogenesis

Supporting Information

Supplementary Material and Methods

Protein expression and purification. PhFap7 and PhNob1 in unlabeled and ^{15}N-labeled form were overexpressed and purified as described previously (1,2). Importantly, UV-spectroscopy and NMR-spectroscopy confirm that PhFap7 does not contain any bound nucleotide after purification. PhS11 was overexpressed overnight at 21°C in *E. coli* (BL21DE3) from a pET11a-derived vector containing a codon-optimized synthetic gene (Entelechon). Following sonication, the cell lysate was cleared by centrifugation and non-thermophilic proteins in the supernatant were precipitated by a 10min 75°C heat-shock. PhS11 was passed over an SP-Sepharose ion-exchange column in 50mM BisTris buffer, pH 6.5, 200 mM NaCl, and eluted with a NaCl gradient. Final purification was achieved through a gel-filtration step using a HiPrep 16/60 Sephacryl S-100 High Resolution column (GE Healthcare) in 50mM BisTris, pH6.5, 50mM NaCl buffer. PhS11ΔC15 was expressed as a fusion protein with an N-terminal histidine tag followed by the SUMO-protein. The fusion protein was initially purified by Ni-NTA-affinity chromatography and the SUMO-tag was cleaved off by the Ulp1-protease leaving a native N-terminus for PhS11ΔC15. PhS11ΔC15 was further purified by gel filtration as described for PhS11. Selectively ^{13}C-threonine/^{15}N-arginine and ^{13}C-proline/^{15}N-α-lysine labeled PhS11 was overexpressed as described previously (1).

RNA synthesis. Fluorescein-labeled helix 23-RNA (fl-h23), helix 40-RNA (h40), helix 45-RNA (h45) and oligo-U_8-RNA (U_8) were obtained commercially (Dharmacon) and de-protected according to the

manufacturer's procedure. Upon folding into monomeric hairpin conformations by heat denaturation followed by snap-cooling on ice the RNAs were exchanged into the required buffers by using microconcentrators (3 kDa MW-cut-off, Vivaspin).

NMR-spectroscopy. All NMR-experiments were recorded at 42°C on Bruker Avance 600, 900 and 950 MHz spectrometers equipped with cryogenic probes in NMR buffer (50 mM BisTris, pH 6.5, 50 mM NaCl and 10% D_2O) using standard pulse sequences. Protein concentrations for all titration experiments were 110 μM. PhNob1 and PhFap7 NMR-signal assignments have been reported previously (1,2). Arginine backbone amide assignments for free PhS11 were obtained by combining the information obtained from the standard set of triple resonance backbone assignment experiments recorded for uniformly ^{13}C,^{15}N-labeled PhS11 and PhS11ΔC15 samples with experiments recorded for selectively ^{13}C-threonine/^{15}N-arginine and ^{13}C-proline/^{15}N-α-lysine labeled PhS11 samples. Combined ^{1}H,^{15}N-chemical shift perturbation values for titration experiments were calculated as described in the literature (3).

Analytical gel filtration. Analytical gel filtration experiments for the detection of protein-protein interactions were carried out using a Superdex S75 10/300 GL (GE) gel filtration column with a flow rate of 1 ml/min on an Äkta purifier system (GEHealthcare) in a 50 mM NaCl, 50 mM BisTris, pH 6.5 buffer at RT. The protein concentration was 10 μM in experiments analyzing the complex formation between PhFap7 and PhS11 or PhS11ΔC15 and 25 μM in experiments analyzing the complex formation between PhFap7 and PhNob1. The total applied sample volume was 100 μl in all cases. Protein elution was followed by recording the adsorption at a wavelength of λ=280 nm since all proteins contain at least one tryptophan.

Yeast-two-hybrid assay. The pADC/pBDC-plasmid system was used (4). PhFap7 and ScFap7 were cloned into the pBDC-plasmid with the DBD-domain fused to their N-termini. PhS11, PhS11ΔC15 and ScS14A were cloned into the pADC-plasmid with the AD-domain fused to their N-termini. All produced plasmids were verified by sequencing. For interaction analysis, the respective plasmid

combinations and controls were co-transformed into the yeast-strain PJ69 (4) and plated onto plasmid selection media (SCD –leu, -trp). Selected colonies were streaked out on interaction media (SCD –leu, -trp, -his, +3 mM 3-amino-1, 2, 4-triazole) and incubated for 7 days at 30°C.

ATPase and adenylate kinase assays. Unless indicated otherwise 50 μM PhFap7, PhS11 and PhNob1 were incubated with either α-[^{32}P]-NTP (for monitoring only the NTPase activity) or γ-[^{32}P]-ATP and 10 mM of unlabeled AMP (simultaneously monitoring the kinase activity and the NTPase activity) in a buffer containing 25 mM Tris-HCl (pH 8.0), 50 mM NaCl, 2 mM $MgCl_2$ and 2 mM DTT at 50 °C for the indicated time points. At 50 μM protein concentration the PhFap7:PhS11 and PhFap7:PhNob1 complexes should be present exclusively given their respective K_Ds. Reactions (20 μL) were prepared on ice and started with the addition of radiolabeled nucleotide. An NTP-concentration of 0.1 mM was used unless stated otherwise. For the single turnover reactions, ATP concentrations as indicated in the corresponding supplementary figure 9 were used. The reaction was stopped by the addition of 2 volumes of 0.5 M EDTA (pH 8.0). Samples (0.8 μL) were spotted onto poly(ethyleneimine)-cellulose TLC plates which were developed in 0.6 M NaH_2PO_4 (pH 3.5). After drying, plates were exposed to a phosphor-imager screen for one hour and signals visualized using the Typhoon PhosphorImager. Quantification was done with the Image Quant Application as supplied by the manufacturer.

Endonuclease assay. Endonuclease assays using PhNob1 were performed as described (5, 6), but 10 μM Nob1 was used and the cleavage reaction stopped after 15 min, where v_{max} was already reached.

Protease protection experiments. Trypsin digestions were performed in 50 mM Tris/HCl, 1 mM $CaCl_2$, pH 7.6 at 4°C using trypsin (Sigma-Aldrich) in a 1:2000 (w/w) enzyme to substrate ratio. Samples were taken at the indicated time points and the reaction was stopped by adding 10 μl SDS loading buffer (1 M Tris/HCl pH6.8, 25% glycerine, 2,5% SDS, 20% β-mercaptoethanol, 0,3 mg/ml bromophenol blue). Samples were analyzed on a 15% SDS-PAGE stained with Coomassie Brilliant Blue.

Fluorescence spectroscopy. For fluoresceine labeling PhFap7 was reduced with DTT, exchanged into a buffer containing 100 mM NaCl, 25 mM Na/HEPES, pH 7.0 using a PD10 desalting column (GE Healthcare) and incubated with a tenfold excess of N(5-fluoresceinyl)maleimide (Sigma Aldrich) for 1 h at RT. The reaction was stopped by addition of 10 mM β-mercaptoethanol and unreacted label was removed by preparative gel filtration. The completion of the labeling reaction was verified using MALDI-mass spectrometry.

All fluorescence measurements were performed at 25 °C using a Fluorolog 3 spectrometer (Horiba Jobin Yvon) equipped with polarizers. Excitation and emission wavelengths were set to 492 nm and 521 nm, respectively. Experiments with fluorescein labeled RNA (fl-h23) were conducted in a buffer containing 50 mM NaCl, 50 mM BisTris, pH 6.5 at an fl-h23 concentration of 50 nM, for all other experiments a buffer of 50 mM NaCl, 0.1 % (v/v) PEG4000, 25 mM Tris/HCl, pH 7.8 was used. fl-PhFap7 concentrations were 10 nM in nucleotide binding experiments, 20 nM for PhNob1 binding experiments and 500 pM for PhS11 binding experiments, which were carried out in the absence or presence of 2 mM ATP, 2mM ATPγS (Jena Bioscience) or 2mM ADP. For measuring the nucleotide affinities to PhFap7-complexes with PhS11 and PhS11ΔC15, PhS11 was added at a concentration of 100 nM and PhS11ΔC15 at a concentration of 1 μM ensuring complete complexation of fl-PhFap7 by its binding partner under these conditions. For all titrations involving nucleotides 2 mM $MgCl_2$ was also added to the buffer. All titrations were performed in triplicate. Binding curves for RNA/PhS11 and fl-PhFap7/PhS11 were fitted to the following equation using Origin 8.1:

$$F = a \cdot \left(\frac{c + r + K_D}{2} - \sqrt{\left(\frac{c + r + K_D}{2} \right)^2 - c \cdot r} \right) + F_0$$

(*F* fluorescence value (either anisotropy or normalized fluorescence intensity), F_0 initial value, K_D dissociation constant, *a* change in fluorescence value, *c* titrant concentration, *r* concentration of fluorescent titrand).

Binding curves of the nucleotide titrations were fitted to the following simplified equation due to the large excess of nucleotides over PhFap7

$$F = a \cdot \frac{c}{c + K_D} + 1$$

(*F* normalized fluorescence intensity, *a* change in fluorescence intensity, *c* nucleotide concentration, K_D dissociation constant)

To determine the dissociation constant of the fl-PhFap7/PhS11ΔC15 complex PhS11 was titrated to a solution of 1 nM fl-Fap7 and 1 µM PhS11ΔC15 and the displacement of PhS11ΔC15 by PhS11 was monitored via the fluorescence intensity. The binding curve was analyzed with Dynafit 4 (7) using the previously determined fl-PhFap7/PhS11 K_D of 22 pM.

To follow the kinetics of the dissociation of the fl-PhFap7/PhS11 complex 20 nM fl-PhFap and 50 nM PhS11 were equilibrated in the absence or presence of 2 mM ATP, 2 mM ADP or 2 mM ATPγS and 5mM $MgCl_2$. The measurement was started after addition of 2 µM unlabeled PhFap7. Fluoresceine anisotropy was measured every 20 s. The shutter was closed between measurements to avoid photobleaching of the fluoresceine chromophore. Anisotropy measurements involving AlF_3 (Sigma Aldrich) were done using 2 mM ADP, 5mM $MgCl_2$ and 10 mM AlF_3. An AlF_3 stock solution was prepared by dissolving AlF_3 in buffer (50 mM NaCl, 0.1 % (v/v) PEG4000, 25 mM Tris/HCl, pH 7.8) by extended preincubation at 60 °C and sonification for 15 minutes prior to the measurements. The anisotropy decay curves were fitted with a monoexponential decay curve ($I=I_0*e^{-k1*t}$). The $t_{1/2}$ times for complex dissociation were calculated as: $t_{1/2} = \ln 2/k1$.

CD-spectroscopy. All CD spectra were recorded using a JASCO J-810 CD-spectrometer. The acquisition parameters for the recording of the melting curves were as follows: bandwith 1 nm, wavelength 220 nm, temperature 30-95 °C, heating rate 1 °C/min, cuvette path length 2 mm. All experiments were done with a protein concentration of 5 µM in CD-buffer (50 mM NaH_2PO_4, 50 mM NaCl, pH 7.0). The PhFap7:PhS11 complex was purified by gel filtration as described above to ensure

a 1:1 stoichiometry of the components. Guanidinium chloride (GnCl) was prepared as a 6 M stock solution in CD-buffer. All melting curves were normalized by division by the absolute value of the minimal CD-Signal [mdeg]. For the determination of the melting temperatures T_m the CD-melting curves were fitted to the following equation using Origin 8.1 as described previously (8):

$$y_{obs} = \frac{y_f + y_u * (\exp\left(\Delta H_m * \left(\frac{1}{T_m} - \frac{1}{T}\right)\right))}{(1 + \exp(\Delta H_m * \left(\frac{1}{T_m} - \frac{1}{T}\right))}$$

(y_{obs} CD signal, y_u CD signal of unfolded protein, y_f CD signal of folded protein, ΔH_m van't Hoff Enthalpie [J], T temperature [°C], T_m melting temperature [°C]). Heat denaturation for both PhS11 and PhFap7 was reversible as ascertained by recording full CD-spectra (195 nm – 300 nm) before and after melting experiments.

Supplementary Figures

A

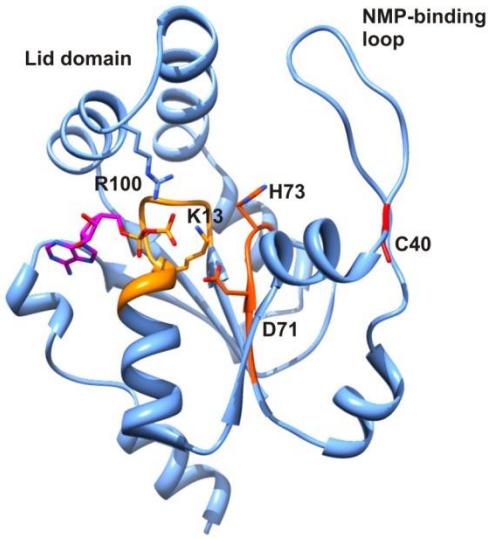

B

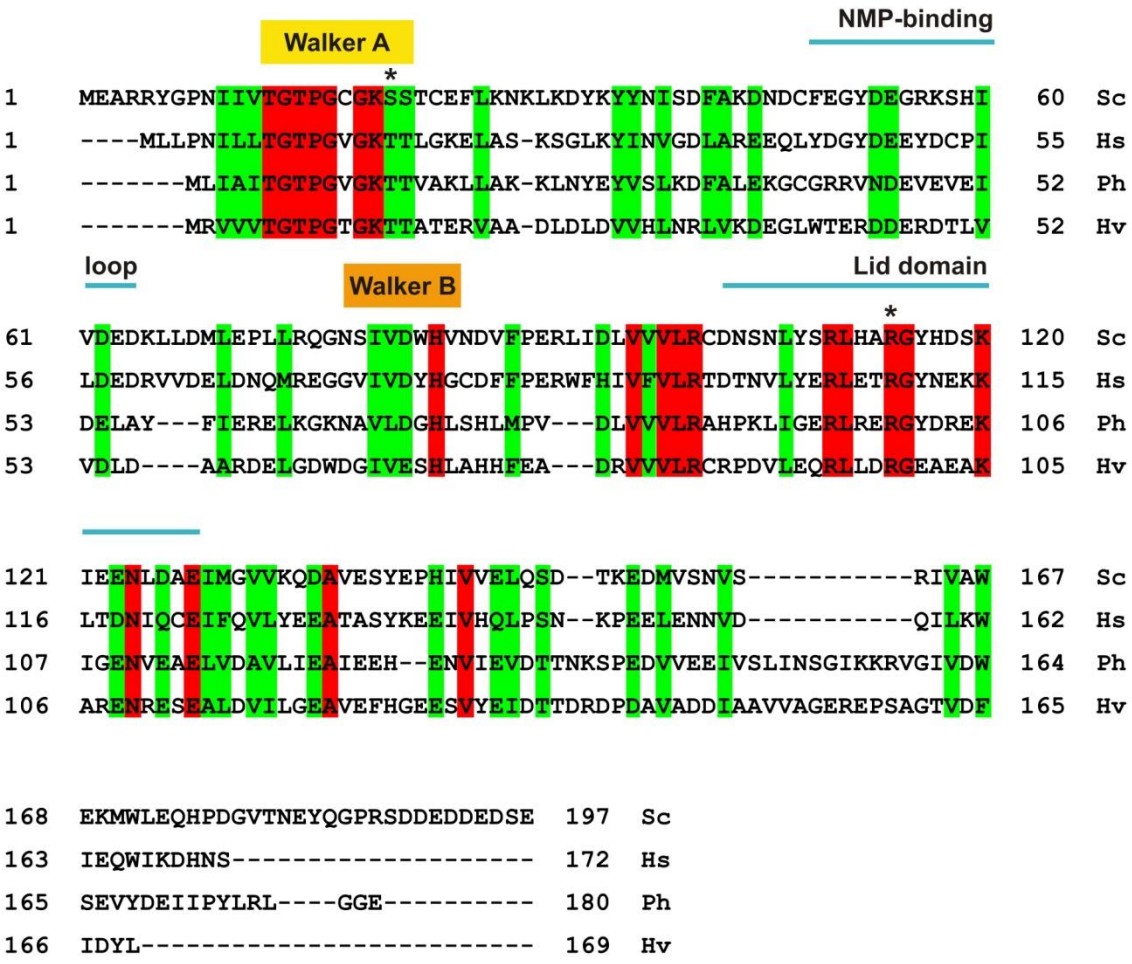

Supplementary Figure 1. Structure elements and conservation of Fap7 between eukaryotes and archaea. (A) Homology model for PhFap7 based on the crystal structure of human ADK6 bound to ADP (pdb [3IIJ]), (9), built using SwissModel (http://swissmodel.expasy.org/). The lid domain important for ATP-binding and the NMP-binding loop typical for adenylate kinase structures are highlighted. The Walker A motif is colored yellow and the Walker B motif is colored orange. The position of cysteine C40 which is surface exposed and used to attach the fluorescent label fluoresceine maleimid to PhFap7 in subsequent experiments is highlighted in red. It is located between the body of the protein and the NMP binding loop. The PhFap7 sequence contains only this single cysteine C40. Functionally important amino acids are shown in stick representation and labeled according to the PhFap7 sequence. (B) Sequence alignment using ClustalW of *Homo sapiens* ADK6 (Hs), *Saccharomyces cerevisiae* Fap7 (Sc), the *Pyrococcus horikoshii* Fap7 homolog (Ph) and the Fap7 homolog from *Haloferax volcanii* (Hv). Identical amino acids are highlighted in red and similar amino acids highlighted in green. A star indicates the position of a conserved serine/threonine in the Walker A motif which is a glycine in all other classes of adenylate kinases and of a conserved arginine in the lid domain which is also important for binding the phosphate groups of the NTP in the NTP-binding site.

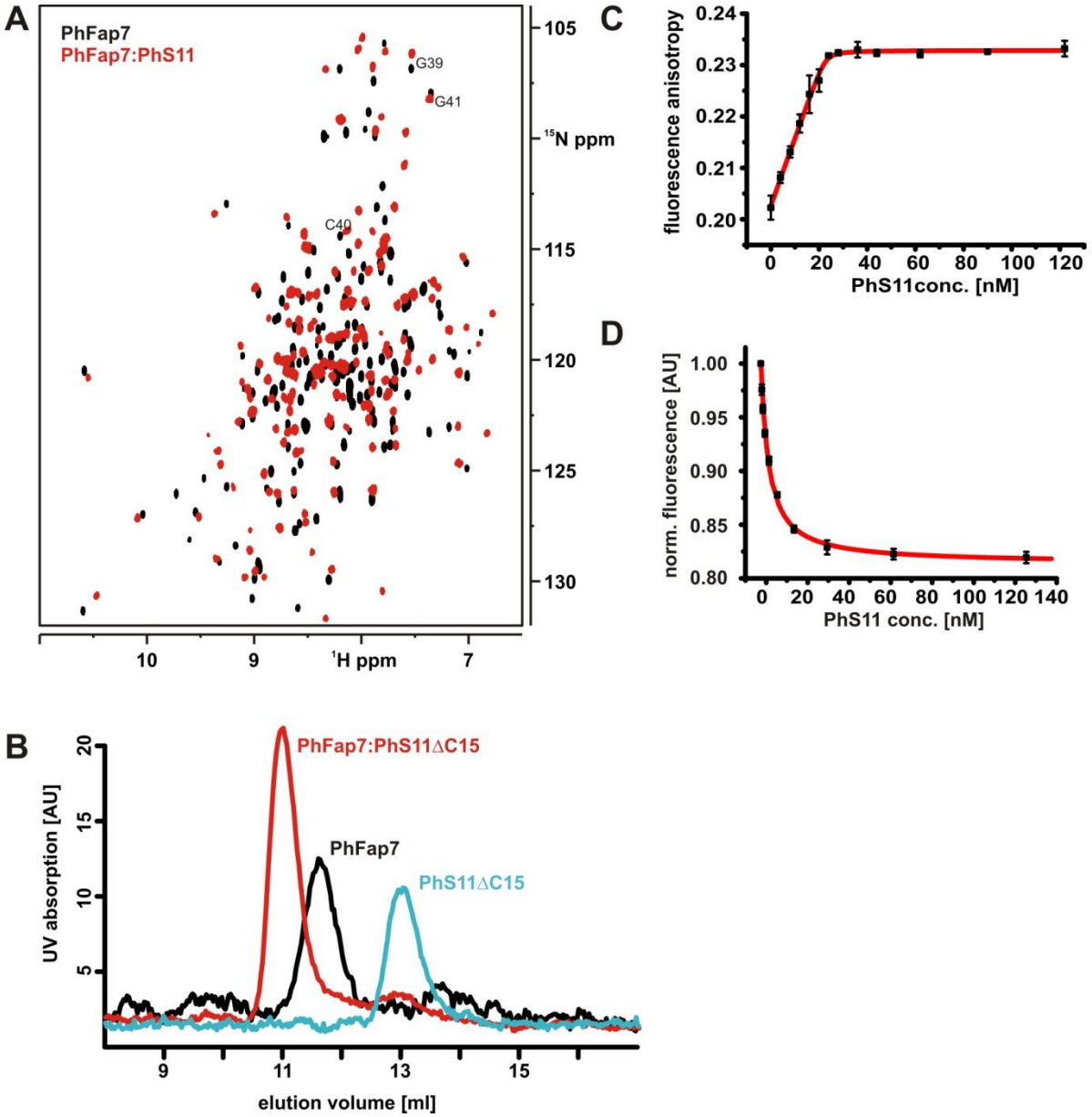

Supplementary Figure 2. Additional characterization of complex formation between PhFap7 and PhS11 or PhS11ΔC15. (A) Overlay of $^{1}H,^{15}N$-TROSY-HSQC-spectra of PhFap7 in its free form (black) and in the presence of one equivalent of unlabeled PhS11 (red). Significant chemical shift changes are observable for the majority of PhFap7-NMR-signals as well as an increase in all signal line widths indicating the formation of a stable PhS11:PhFap7-complex in slow exchange on the NMR time scale. Addition of further equivalents of PhS11 did not induce additional spectral changes. The extensive chemical shift changes observed for PhFap7 upon complex formation are not limited to a continuous surface of PhFap7. This indicates that PhS11 also leads to allosteric changes in the structure of PhFap7. Unfortunately, the PhFap7:PhS11 complex transiently aggregates at concentrations above

120 μM as seen by increasing line widths at higher concentrations precluding NMR resonance assignments of PhFap7 in the complex and a chemical shift based mapping of the PhS11-binding site. Furthermore, the backbone amide signal positions for G39, C40 and C41 are labeled in the spectrum. C40 corresponds to the site of fluoresceine incorporation. Only minor chemical shift changes are observed for these residues upon PhS11 addition indicating that fluorescence labeling does not interfere with complex formation. (B) Formation of a stable 1:1 complex between PhFap7 and PhS11ΔC15 as observed in analytical gel filtration experiments. The elution profiles for free PhFap7 and PhS11ΔC15 are shown in black and blue, respectively. For a 1:1 mixture of the two proteins the red elution profile is obtained which contains a single peak at an earlier elution time indicating complex formation. (C) Complex formation between fluoresceine-labeled PhFap7 (fl-PhFap7) and PhS11 investigated by fluorescence anisotropy experiments. Titration of fl-Phfap7 with increasing amounts of PhS11 leads to an increase of the observed fluorescence anisotropy indicating the formation of an fl-PhFap7:PhS11 complex. However, at the concentrations of fl-PhFap7 required to obtain a reasonable signal-to-noise-ratio in the fluorescence anisotropy measurements (10 nM) saturation already occurred at a 1:1 molar ratio of fl-PhFap7 and PhS11 in agreement with the very high affinity between the two proteins. (D) Indirect determination of the K_D for the PhFap7:PhS11ΔC15 interaction in a competition experiment using PhS11 induced fluorescence quenching. PhS11ΔC15 does not induce quenching of the fluoresceine fluorescence of fl-PhFap7. Titration of fl-PhFap7 (1nM) with full-length PhS11 in the presence of a 1000fold excess of PhS11ΔC15 (1μM) yields a saturation curve allowing to extract the affinity of PhS11ΔC15 for PhFap7 using the known K_D of PhS11 as described in supplementary material and methods.

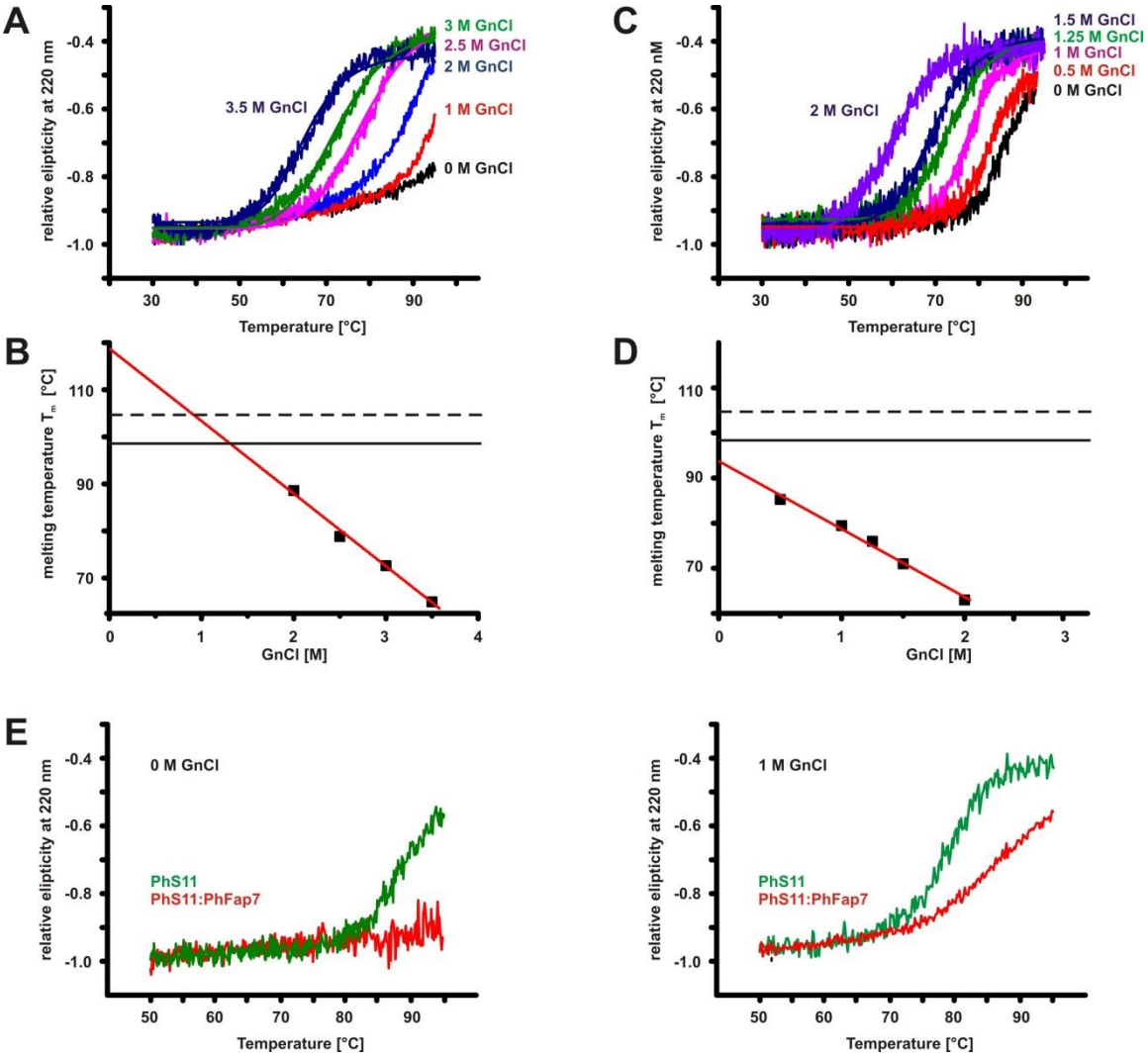

Supplementary Figure 3. PhFap7 stabilizes PhS11 against thermal denaturation. (A) Normalized CD-melting curves at 220 nm of PhFap7 at different guanidinium chloride (GnCl) concentrations. At GnCl-concentrations < 2M only partial denaturation of PhFap7 is observed. (B) Extrapolation of the melting temperature T_m for free PhFap7 at 0M GnCl by linear regression. Only melting curves at GnCl-concentrations > 2M were considered where complete denaturation of PhFap7 was observed. The linear regression resulted in a melting temperature for PhFap7 at 0M GnCl of 118°C well above both the optimal growth temperature of 98°C (solid black line) and the maximal growth temperature of 104°C (dashed black line) for *Pyrococcus horikoshii*. (C) Normalized CD-melting curves at 220 nm of PhS11 at different GnCl-concentrations. (D) Extrapolation of the melting temperature T_m for free PhS11 at 0M GnCl by linear regression. The linear regression resulted in a melting temperature for PhFap7 at 0 M GnCl of 93°C which is below the optimal growth temperature of 98°C (solid black line)

and the maximal growth temperature of 104°C (dashed black line) for *Pyrococcus horikoshii*. (E) Comparison of the melting curves for free PhS11 (green) and the PhS11:PhFap7-complex (red) at 0M GnCl (left) and 1M GnCl (right). For the PhS11:PhFap7-complex the onset of melting is significantly delayed in comparison to free PhS11. At higher GnCl concentrations complex dissociation and melting of the free components contribute to the observed melting curves and no melting temperature for the PhFap7:PhS11-complex can be determined.

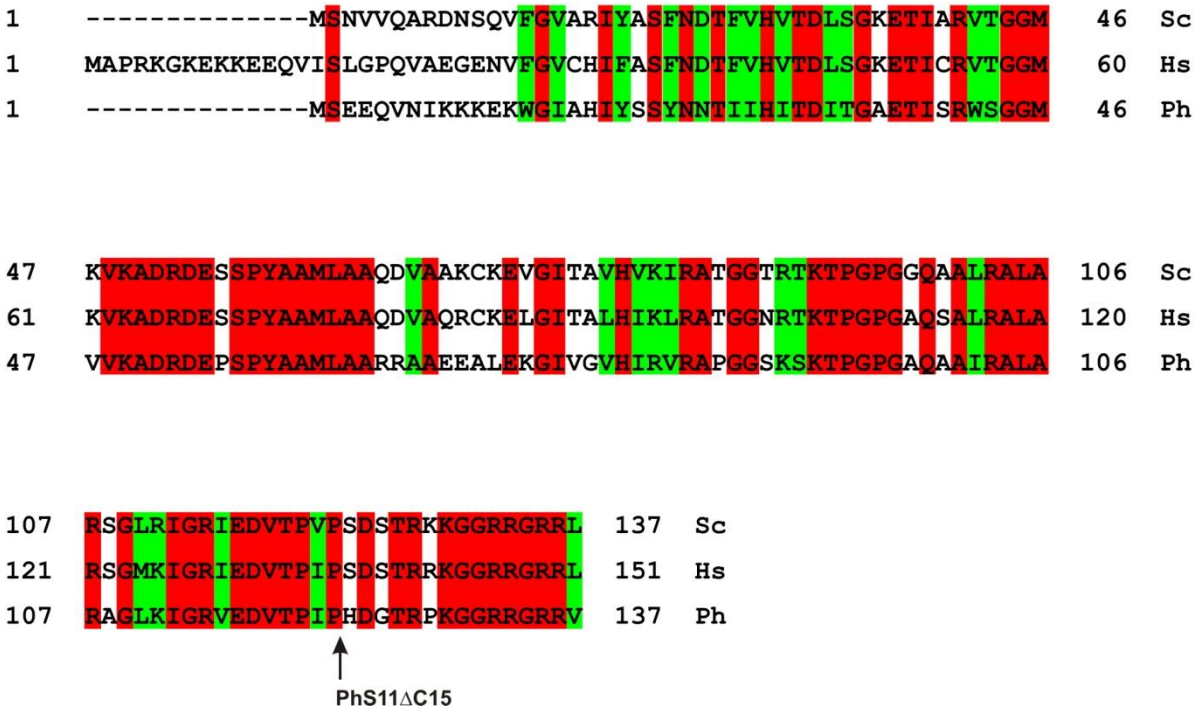

Supplementary Figure 4. Sequence conservation for ribosomal protein S14 homologs between eukaryotes and *Pyrococcus horikoshii*. A sequence alignment between human ribosomal protein S14 (Hs), *Saccharomyces cerevisiae* ribosomal protein S14A (ScS14A) (Sc) and *P. horikoshii* S11 (PhS11) (Ph) is shown. Identical amino acids are highlighted in red and similar amino acids in green. The C-terminus is among the most conserved regions of the protein. The site for the deletion of the C-terminus in PhS11ΔC15 is also indicated.

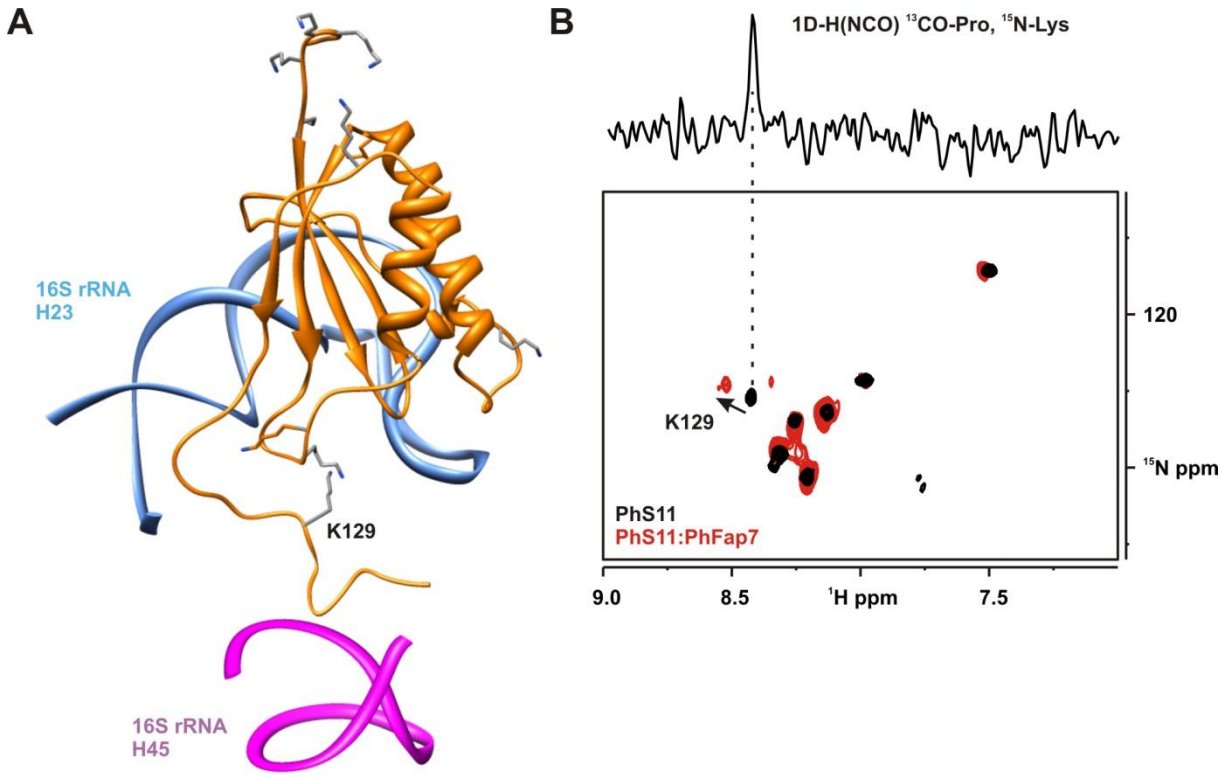

Supplementary Figure 5. Further characterization of the PhS11:PhFap7 interaction by NMR-spectroscopy. (A) Location of the lysine residues (with K129 pointed out) in a structural model of PhS11 bound to the small ribosomal subunit based on the X-ray-structure of the small ribosomal subunit of *Tetrahymena thermophila*. The lysine side chains are shown in stick representation whereas the remainder of the protein is shown as a secondary structure cartoon. In contrast to the arginine residues of PhS11 (Figure 1) the lysine residues are not directly located in the RNA-binding sites of PhS11. (B) Overlay of ^{1}H,^{15}N-TROSY-HSQC-spectra of selectively ^{15}N-lysine, ^{13}CO-proline labeled PhS11 in its free form (black) and bound to unlabeled PhFap7 (red). Only one of the lysine backbone amide signals of PhS11 shifts upon PhFap7 addition as indicated by the arrow and no new signals appear. The shifting signal is identified as belonging to lysine 129 in an 1D-H(NCO)-experiment (dashed line) since lysine 129 is the only lysine preceded by a proline residue (P128) in the sequence of PhS11. This further supports the interaction between PhFap7 and the C-terminal tail of PhS11.

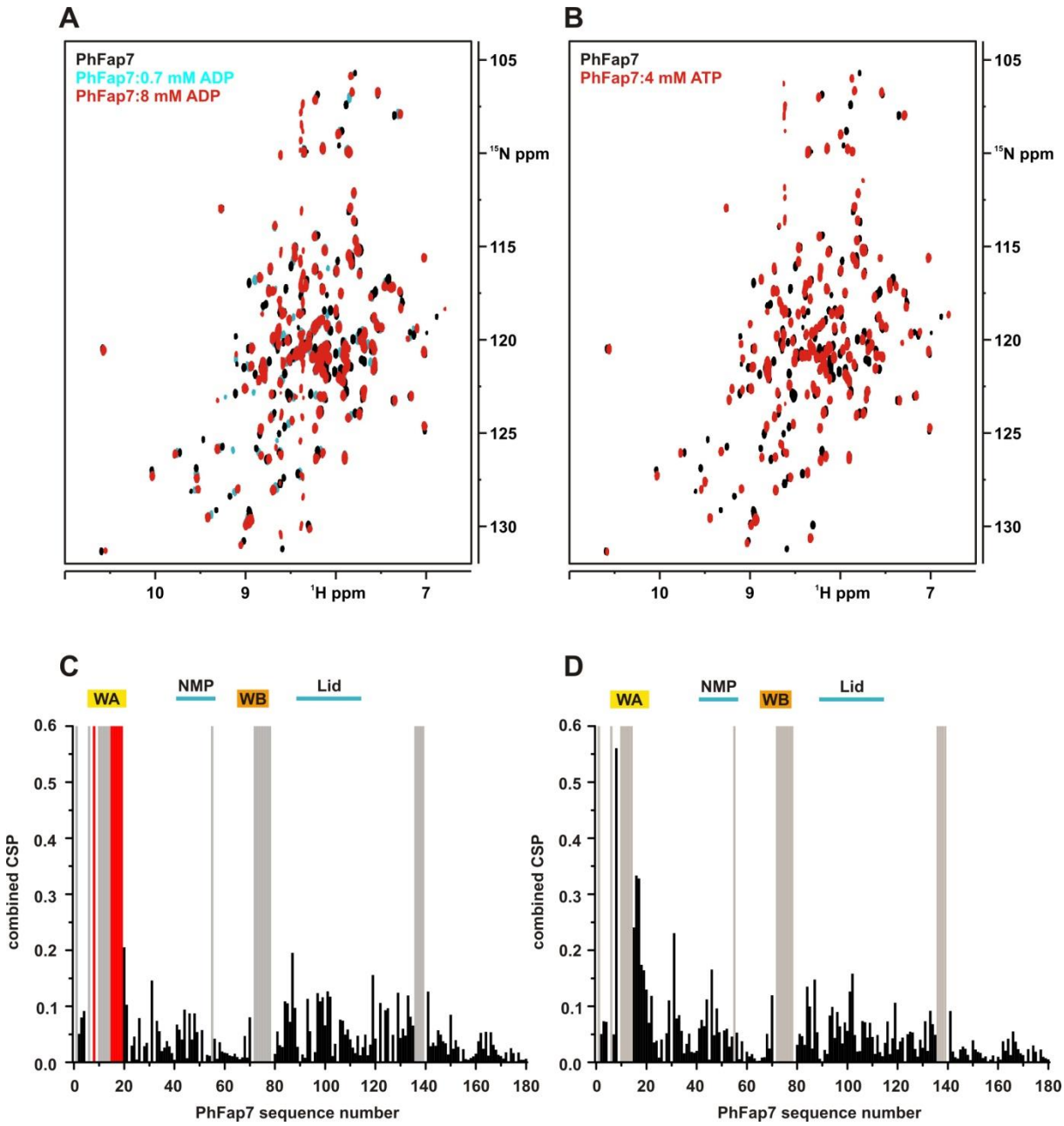
A
PhFap7
PhFap7:0.7 mM ADP
PhFap7:8 mM ADP
105
115
120
125
130
^{15}N ppm
10
9
^{1}H ppm
7
B
PhFap7
PhFap7:4 mM ATP
105
115
120
125
130
^{15}N ppm
10
9
^{1}H ppm
7
C
WA
NMP
WB
Lid
combined CSP
0.0
0.1
0.2
0.3
0.4
0.5
0.6
0
20
40
60
80
100
120
140
160
180
PhFap7 sequence number
D
WA
NMP
WB
Lid
combined CSP
0.0
0.1
0.2
0.3
0.4
0.5
0.6
0
20
40
60
80
100
120
140
160
180
PhFap7 sequence number

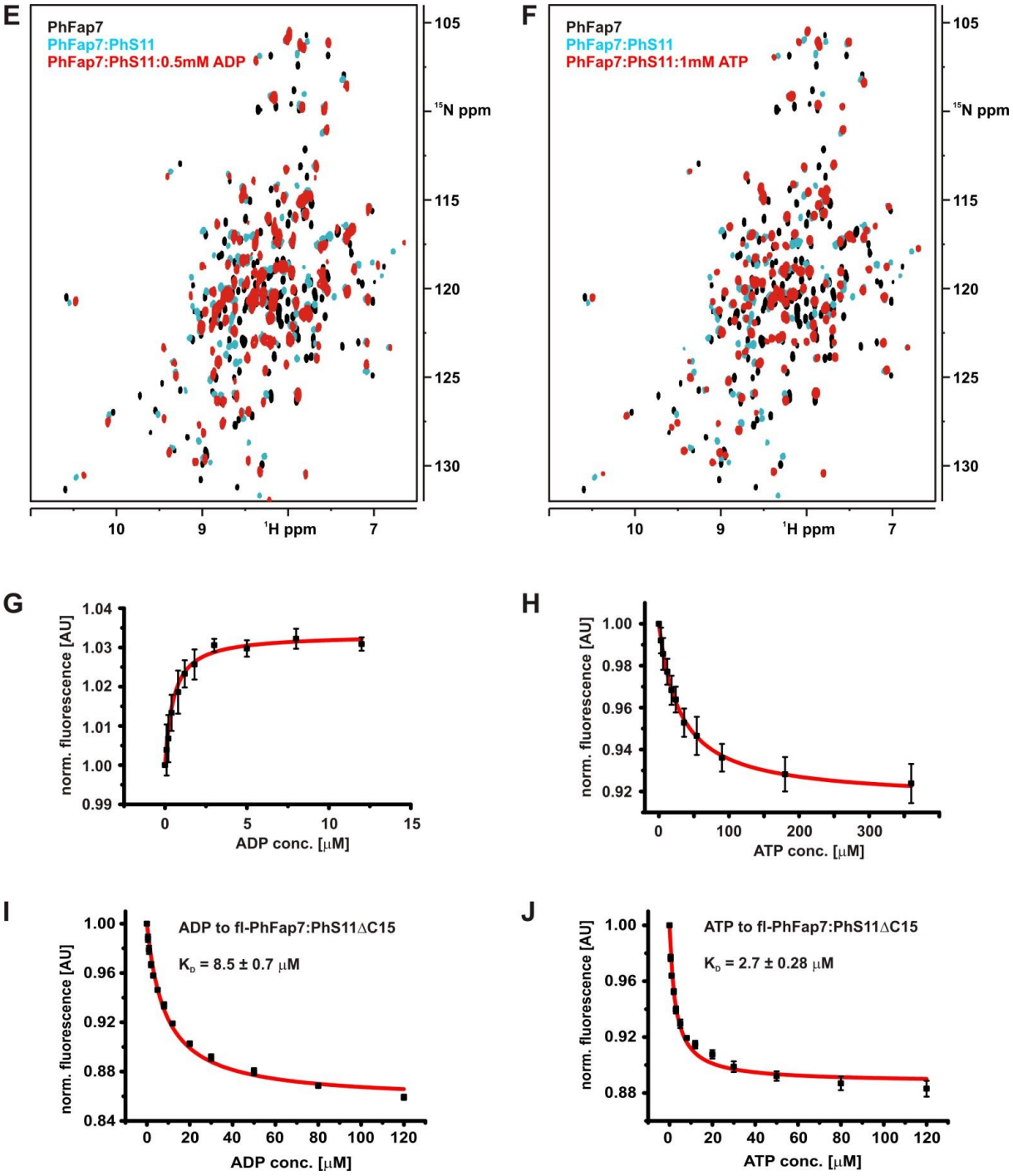

Supplementary Figure 6. Nucleotide binding to PhFap7 and the PhFap7:PhS11 complex. (A) Overlay of $^{1}H,^{15}N$-TROSY-HSQC-spectra of PhFap7 in its free form (black) and in the presence of increasing amounts of ADP (blue and red, respectively). (B) Overlay of $^{1}H,^{15}N$-TROSY-HSQC-spectra of PhFap7 in its free form (black) and in the presence of saturating amounts of ATP (red). (C) Combined $^{1}H,^{15}N$-chemical shift perturbations (3) for PhFap7 in the presence of saturating amounts of ADP (8 mM) and in the absence of Mg^{2+} plotted against the sequence of PhFap7. Chemical shift perturbations are

plotted as black bars whereas red bars indicated resonances that broaden out and gradually disappear upon nucleotide binding. Gray bars indicate missing assignments for the free PhFap7 (1) due to intrinsic dynamical disorder. The most pronounced effects of ADP binding are observed for residues in the vicinity of the Walker A motif and residues in the lid domain indicating that ADP preferentially binds to the NTP-binding site of PhFap7 comprised of the Walker motifs and the lid domain and not the NMP-binding site (NMP-binding loop and residues 35-40). (D) Combined $^{1}H,^{15}N$-chemical shift perturbations (4) for PhFap7 in the presence of saturating amounts of ATP (4 mM) and in the absence of Mg^{2+} plotted against the sequence of PhFap7. Chemical shift perturbations are plotted as black bars whereas gray bars indicate missing assignments for the free PhFap7 (1) due to intrinsic dynamical disorder. Again, the most prominent chemical shift perturbations are observed for residues in the vicinity of the Walker A motif and the lid domain. (E) ADP-binding to the PhFap7:PhS11 complex. Overlay of $^{1}H,^{15}N$-TROSY-HSQC-spectra of ^{15}N-labeled PhFap7 bound to unlabeled PhS11 in the absence (black) and in the presence (red) of saturating amounts of ADP (0.5 mM) and of free PhFap7 (blue). The chemical shift differences and differences in line-widths suggest that ADP stably binds to the complex and does not induce PhFap7:PhS11-complex dissociation. (F) ADP-binding to the PhFap7:PhS11 complex. Overlay of $^{1}H,^{15}N$-TROSY-HSQC-spectra of ^{15}N-labeled PhFap7 bound to unlabeled PhS11 in the absence (black) and in the presence (red) of saturating amounts of ATP (1.0 mM) and of free PhFap7 (blue). The chemical shift differences and differences in line-widths suggest that ATP stably binds to the complex and does not induce PhFap7:PhS11-complex dissociation. (G) and (H) Enlarged versions of the fluorescence quenching titration curves for the determination of the ADP and ATP-affinities of the PhFap7:PhS11-complex in the presence of Mg^{2+} shown in Figure 3A. It should be noted that in contrast to ATP-binding, ADP-binding does not induce fluorescence quenching but an increase in fluorescence. Similarly, binding of full-length PhS11 to the ADP:PhFap7 complex leads to an increased fluorescence whereas the addition of PhS11 to the ATP:PhFap7 complex induces fluorescence quenching. This hints at different structures of PhFap7 when bound to ADP and PhS11 or bound to ATP and PhS11. (I) and (J) Fluorescence quenching titration experiments for the determination of the ADP and ATP affinities of the PhFap7:PhS11ΔC15-

complex. In the absence of the C-terminus both nucleotides induce fluorescence quenching indicating that it is the very C-terminus of PhS11 which interacts differently with PhS11 in the two different nucleotide bound states.

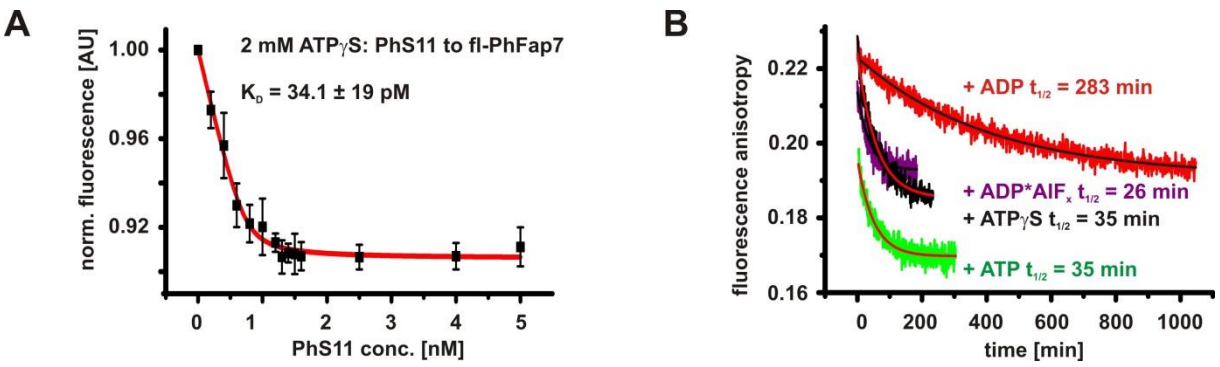

Supplementary Figure 7. Influence of ATPγS on the PhFap7:PhS11 complex stability. (A) Fluorescence quenching titration curve for the determination of the PhS11-affinity for PhFap7 in the presence of the ATP-analog ATPγS and Mg^{2+}. (B) Dissociation kinetics of the fl-PhFap7:PhS11 complex upon addition of a 100 fold excess of unlabeled PhFap7 in the presence of Mg^{2+} and the ATP-analog ATPγS (black) and the transition state analog ADP*AlF_x (magenta), observed by fluorescence anisotropy. The dissociation curves in the presence of ADP (red) and ATP (green) from figure 3 are shown for comparison.

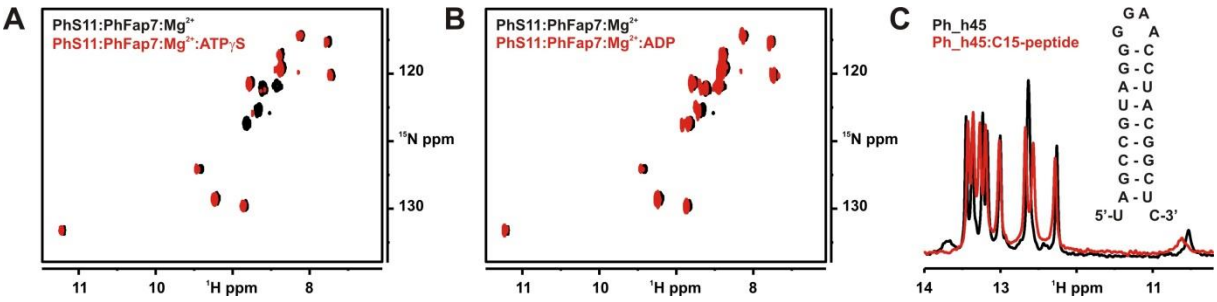

Supplementary Figure 8. Impact of nucleotide binding to the PhS11:PhFap7 complex on the C-terminal tail of PhS11. (A) Effect of ATPγS-addition (2mM) in the presence of 2mM Mg^{2+} on the ^{15}N-HSQC-spectrum of selectively ^{15}N-arginine labeled PhS11 bound to unlabeled PhFap7. Upon nucleotide addition four backbone amide signals which can be tentatively assigned to the extreme C-terminal tail of PhS11 disappear or diminish strongly in their intensity. This indicates that the backbone amide groups of the four terminal arginines become strongly solvent exposed in the presence of ATPγS in agreement with the proposed release of the C-terminal tail of PhS11 from the interaction with PhFap7. However, they are protected from solvent exchange in the nucleotide-free PhS11:PhFap7-complex in agreement with a stable interaction of the C-terminal peptide of PhS11 with PhFap7 in the absence of nucleotide (Fig. 1G). Importantly, all other arginine backbone amide signals do not show significant chemical shift changes demonstrating that the interaction between the globular body of PhS11 and PhFap7 stays intact upon ATPγS-addition. ATPγS had to be used in place of ATP to prevent nucleotide hydrolysis under the conditions used for recording the NMR-experiments (42°C, presence of Mg^{2+}, 90 min acquisition time). (B) Effect of ADP-addition (2mM) in the presence of 2mM Mg^{2+} on the ^{15}N-HSQC-spectrum of selectively ^{15}N-arginine labeled PhS11 bound to unlabeled PhFap7. ADP-binding to the complex induces only small chemical shift changes for the C-terminal backbone amide signals but no reduction in signal intensities in contrast to ATPγS. Thus, in the presence of ADP the C-terminal tail of PhS11 remains stably bound to PhFap7. (C) The C-terminal peptide of PhS11 (C15-peptide: NH_2- HDGTRPKGGRRGRRV-COOH) is able to bind the isolated helix45-RNA (Ph-h45, right). Comparison of imino proton 1D-NMR-spectra of free Ph-h45

(black) and Ph-h45 in the presence of 2.5 equivalents of the C15-peptide (red). Small chemical shift changes are observed for some of the imino protons of Ph-h45 in the presence of the peptide indicative of binding in the fast-exchange regime on the NMR-time scale in agreement with a weak interaction between the RNA and the peptide.

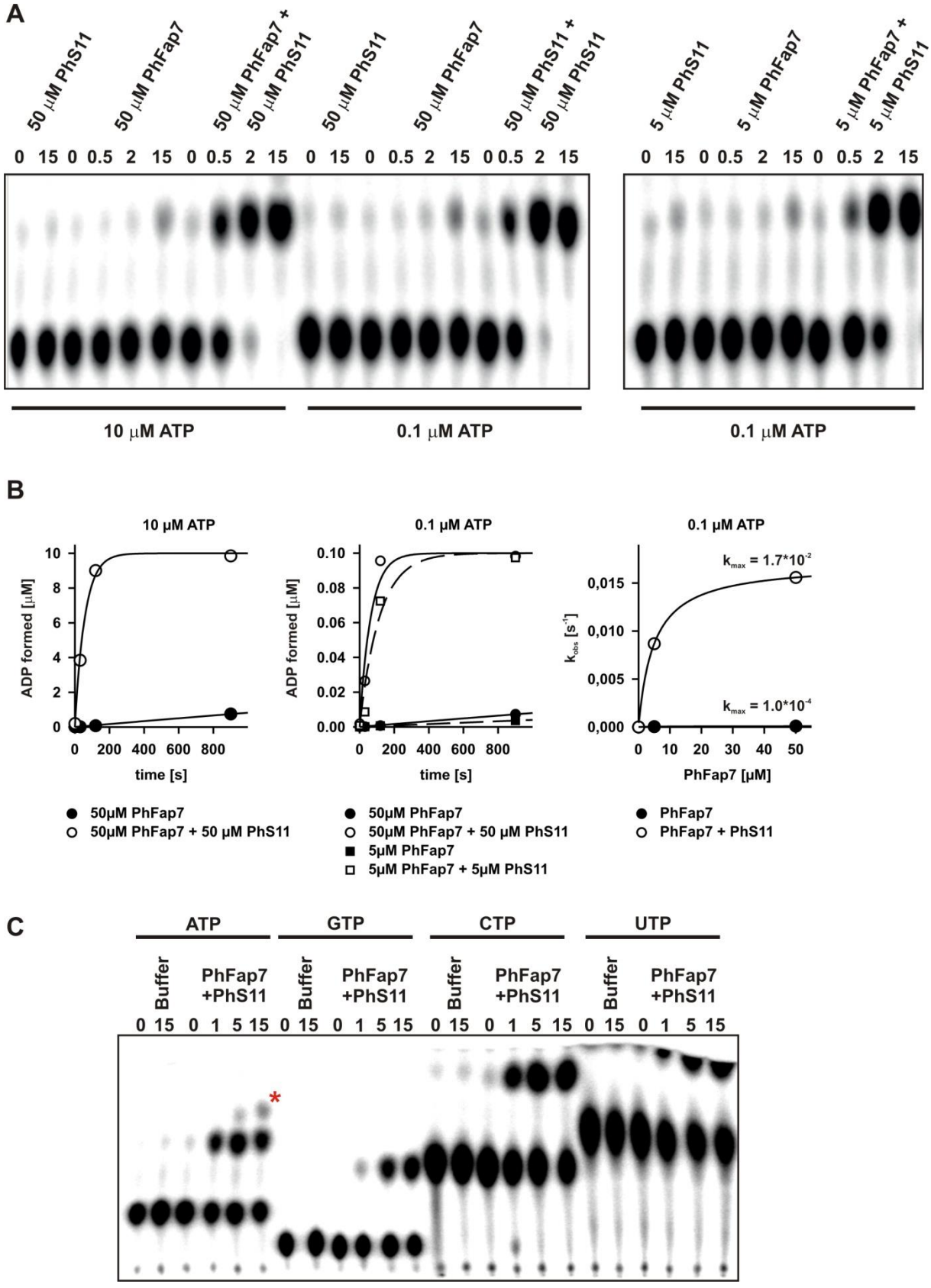

Supplementary Figure 9. Further characterization of the enzymatic activity of PhFap7. (A) Thin-layer chromatographic analysis of the ATPase activity of PhFap7 and the PhFap7:PhS11 complex under conditions where only the ATPase reaction can occur due to the absence of AMP. The nucleotide and

protein concentrations were chosen as indicated to essentially observe single turnover kinetics. In all lanes the lower band represents the substrate α-^{32}P-labeled ATP and the upper band the product α-^{32}P-labeled ADP. (B) Quantitative analysis of the reaction time courses seen in (A) according to equations (1) and (3) in reference (10). Under the chosen conditions the k_{max} values correspond to the chemical step of the reaction (k_{cat}) (10). (C) General NTPase activity of the PhFap7:PhS11 complex. The other three naturally occurring NTPs are converted to NDPs with similar efficiency. The substrate in all four cases is the α-^{32}P-labeled NTP. In all lanes the lower band corresponds to the substrate NTP whereas the upper band corresponds to the product α-^{32}P-labeled NDP. An asterisk in the ATPase reaction marks the occurrence of α-^{32}P-labeled AMP which is the product of the reverse kinase reaction converting two ADPs into ATP and AMP. This reaction occurs simultaneously with the ATPase reaction once enough ADP has accumulated.

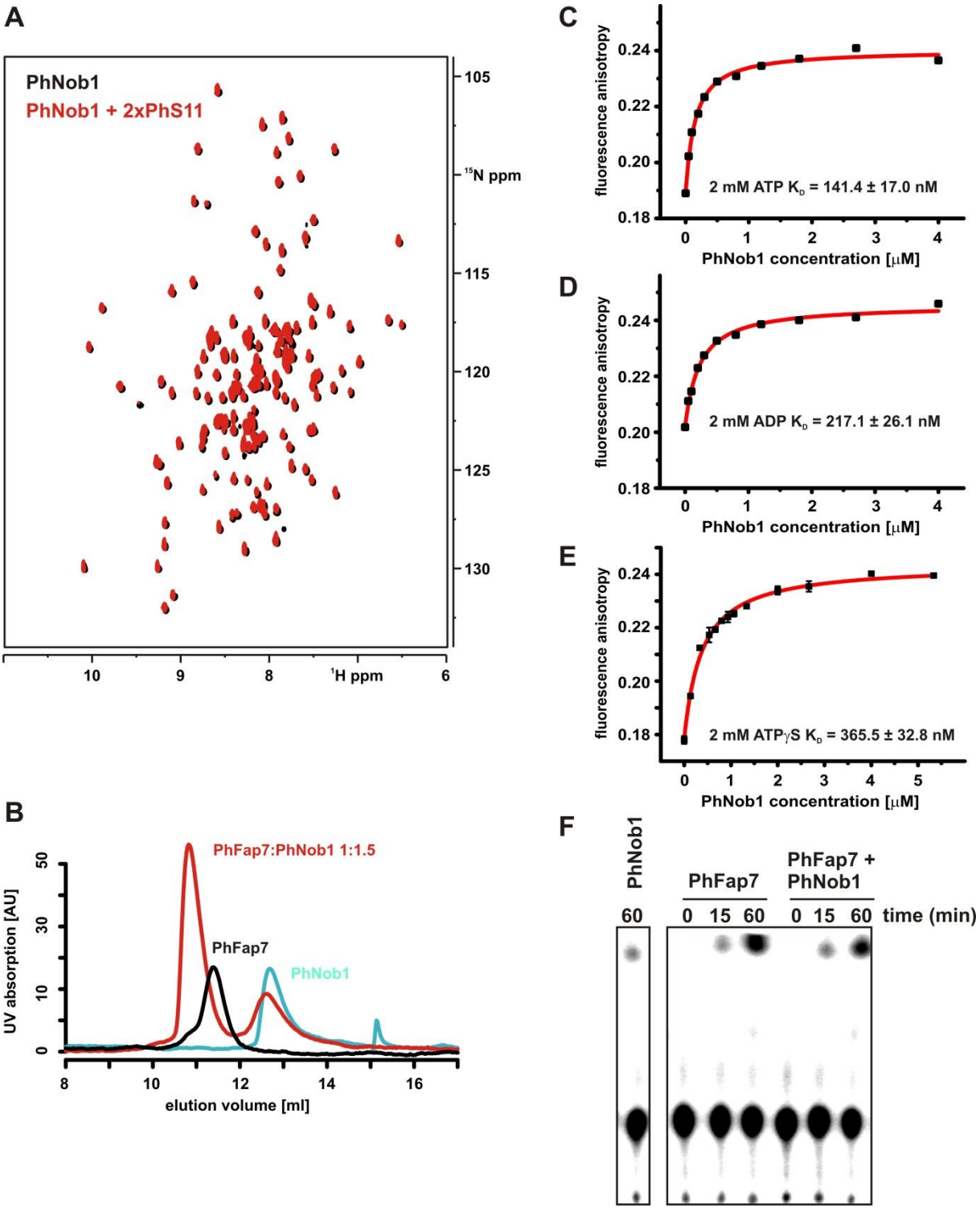

Supplementary Figure 10. PhNob1 binds to PhFap7 but not to PhS11. (A) Overlay of ^{1}H,^{15}N-TROSY-HSQC-spectra of PhNob1 in its free form (black) and in the presence of two equivalents of unlabeled PhS11 (red). The two spectra are virtually identical indicating that PhNob1 and PhS11 do not interact directly. (B) Analysis of the interaction between PhNob1 and PhFap7 by analytical gel filtration experiments. Elution profiles for free PhNob1, free PhFap7 and a 1:1.5 mixture of PhFap7 and

PhNob1 are shown in blue, black and red, respectively. (C), (D) and (E) The presence of ATP, ADP and ATPγS does not significantly influence the affinity of fl-PhFap7 for PhNob1 as seen from fluorescence anisotropy titration experiments where fl-PhFap7 is titrated with increasing amounts of PhNob1 in the presence of each nucleotide and 2 mM Mg^{2+}. The obtained K_Ds in the presence of all three nucleotides are very similar to each other and to the K_D in the absence of nucleotide (Figure 4). (F) Thin layer chromatographic analysis of the ATPase reaction of PhFap7 in the absence and the presence of PhNob1 using γ-^{32}P-ATP as the substrate. In contrast to PhS11 PhNob1 is not able to stimulate the ATPase-activity of PhFap7. In all lanes the lower band corresponds to the substrate γ-^{32}P-ATP and the upper band to the product γ-^{32}P-P_i.

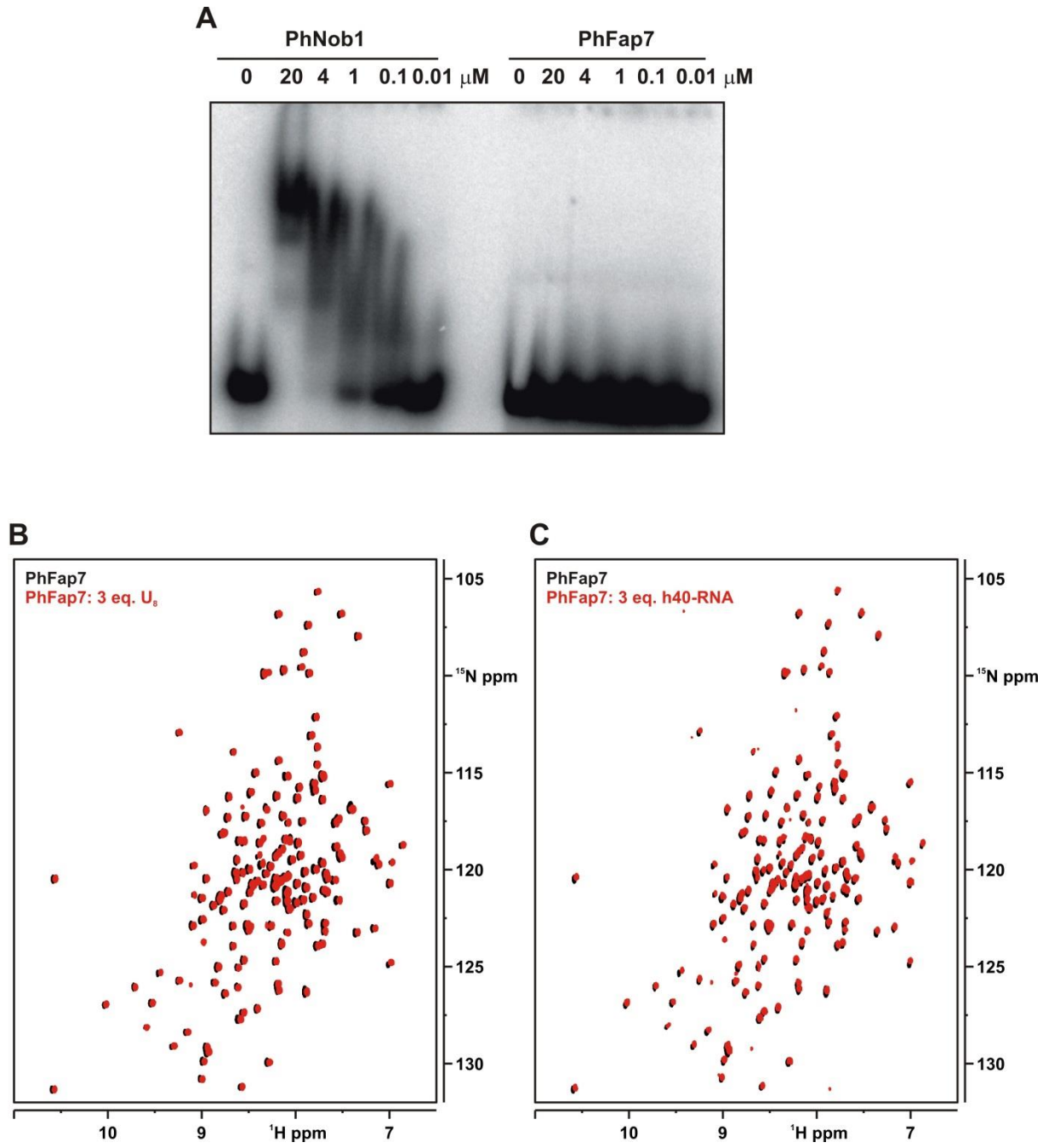

Supplementary Figure 11. PhFap7 does not interact with RNA. (A) In contrast to PhNob1 (left), PhFap7 does not bind to the RNA-substrate used in PhNob1-cleavage assays (6) in an electrophoretic mobility shift assay (EMSA). Thus, PhFap7 cannot inhibit RNA-cleavage by PhNob1 indirectly by blocking the PhNob1-cleavage site on the RNA due to PhFap7-RNA interactions. EMSA-assays require comparatively high affinities between RNA and protein to result in clear mobility shifts. However, PhFap7 does not even interact weakly with single-stranded RNA (oligo-U_8-RNA) or double-stranded

hairpin (h40-RNA) (6) RNA as seen in NMR-titrations of ^{15}N-PhFap7 with U_8-RNA (B) or h40-RNA (C). The ^{15}N-TROSY-HSQC-spectrum of PhFap7 does not change in the presence of either RNA (B,C).

Supplementary References

1. Hellmich UA, Wöhnert J (2012) Backbone resonance assignments for a homolog of the essential ribosome biogenesis factor Fap7 from P. horikoshii in its nucleotide-free and -bound forms. *Biomol NMR Assign* doi:10.1007/s12104-012-9423-9.

2. Veith T et al. (2012) Backbone and side chain NMR resonance assignments for an archaeal homolog of the endonuclease Nob1 involved in ribosome biogenesis. *Biomol NMR Assign* 6:47-50.

3. Mulder FAA, Schipper D, Bott R, Boelens R (1999) Altered flexibility in the substrate-binding site of related native and engineered high alkaline Bacillus subtilisins. *J Mol Biol* 292:111–123.

4. Millson SH, Truman AW, Piper PW (2003) Vectors for N- or C-terminal positioning of the yeast Gal4p DNA binding or activator domains. *Biotechniques* 35:60-64.

5. Pertschy S et al. (2009) RNA helicase Prp43 and its co-factor Pfa1 promote 20S to 18S rRNA processing catalyzed by the endonuclease Nob1. *J Biol Chem* 284:35079-35091.

6. Veith et al. (2012) Structural and functional analysis of the archaeal endonuclease Nob1. *Nucleic Acids Res* 40:3259-3274.

7. Kuzmic P (1996) Program DYNAFIT for the analysis of enzyme kinetic data: application to HIV proteinase *Anal Biochem* 237:260-273.

8. Brumano MH, Rogana E, Swaisgood HE (2000) Thermodynamics of unfolding of beta-trypsin at pH 2.8. Arch Biochem Biophys 382(1):57-62.

9. Drakou CE et al. (2012) hCINAP is an atypical mammalian nuclear adenylate kinase with an ATPase motif: structural and functional studies. *Proteins* 80: 206-220.

10. Peluso P, Shan S, Nock S, Herschlag D, Walter P (2001) Role of SRP RNA in the GTPase cycles of Ffh and FtsY. *Biochemistry* 40:15224-15233.